Received: 23 February 2021 | Revised: 22 July 2021 | Accepted: 30 July 2021

DOI: 10.1002/aoc.6409

FULL PAPER

Applied Organometallic Chemistry WILEY

Core-shell structured magnetite silica-supported hexatungstate: A novel and powerful nanocatalyst for the synthesis of biologically active pyrazole derivatives

Ramin Nemati | **Dawood Elhamifar** | **Ali Zarnegaryan** | **Masoumeh Shaker**

Department of Chemistry, Yasouj University, Yasouj, Iran

Correspondence
Dawood Elhamifar, Department of Chemistry, Yasouj University, Yasouj 75918-74831, Iran.
Email: d.elhamifar@yu.ac.ir

Funding information
Iran National Science Foundation; Yasouj University

Abstract

This article describes the synthesis of a novel core-shell structured magnetic silica-supported hexatungstate (Fe_3O_4@SiO_2-NH_3[W_6O_{19}]) nanocatalyst through immobilization of hexatungstate on amine-modified magnetic silica nanoparticles. The physicochemical properties of Fe_3O_4@SiO_2-NH_3[W_6O_{19}] were investigated by using Fourier transform infrared (FT-IR) spectroscopy, powder X-ray diffraction, vibrating sample magnetometer, wide-angle PXRD, scanning electron microscopy, transmission electron microscopy, and energy-dispersive X-ray spectroscopy analyses. The Fe_3O_4@SiO_2-NH_3[W_6O_{19}] nanocatalyst was used as a powerful and heterogeneous catalyst in the synthesis of pyrazole derivatives. This novel catalyst was reused at least seven times without loss of its activity.

KEYWORDS

core-shell, nanocatalyst, polyoxometalate, pyrazole

1 | INTRODUCTION

Pyrazole and its derivatives are among the five-membered heterocycles constituting a class of compounds particularly effective in organic synthesis. These have received considerable attention due to their wide range of medicinal properties and biological activity.[1,2] Some biological activities of pyrazoles are antioxidant,[3] antibacterial,[4,5] analgesic,[6] antitumor,[7,8] cardiovascular,[9] anticonvulsant,[10] and so on. Although many studies have been reported for the synthesis of pyrazole products using homogeneous and heterogeneous catalysts, most of these reports suffer from restrictions of high temperature and high pressure and the use of environmentally harmful organic solvents.[11,12] Therefore, it is very important to develop a clean catalytic process for the efficient synthesis of pyrazoles.

Polyoxometalates are a class of metals with highest oxidation state containing oxo-ligands. Due to the unique properties of polyoxometalates such as diversity in structure, high thermal stability, high surface charge distribution, and resistance toward oxidative conditions, they have been thoroughly considered as catalyst either under heterogeneous or homogeneous conditions.[13–16] Among different structures of polyoxoanions, Lindqvist one with formula of $[M_6O_{19}]^{n-}$ (M = W, Mo, Ta, V, and Nb) is more considered.[17] As an individual metal oxide cluster, the Lindqvist hexatungstate is a very good candidate for the construction of hybrid materials.

Facing with the requirement of sustainable expansion, many efforts have been made to design and preparation of polyoxometalate-based hybrid materials, not only due to their appealing architectures[18,19] but also owing to their potential applications in the catalysis,

surface and interface science, magnetic chemistry, materials science, and analytical chemistry.[15,16,20–23]

On the other hand, in recent years, nanocomposites have attracted a lot of attention due to their wide applications in various fields such as photocatalysts[24,25] and catalysts,[26–33] lithium batteries,[34] biomedical,[35] solar cells,[36] and sensors.[37] Magnetic core-shell structured nanomaterials, as a special class of nanocomposites, are particularly important between researchers. Among these, the Fe_2O_3@SiO_2 NPs with Fe_3O_4 core and silica

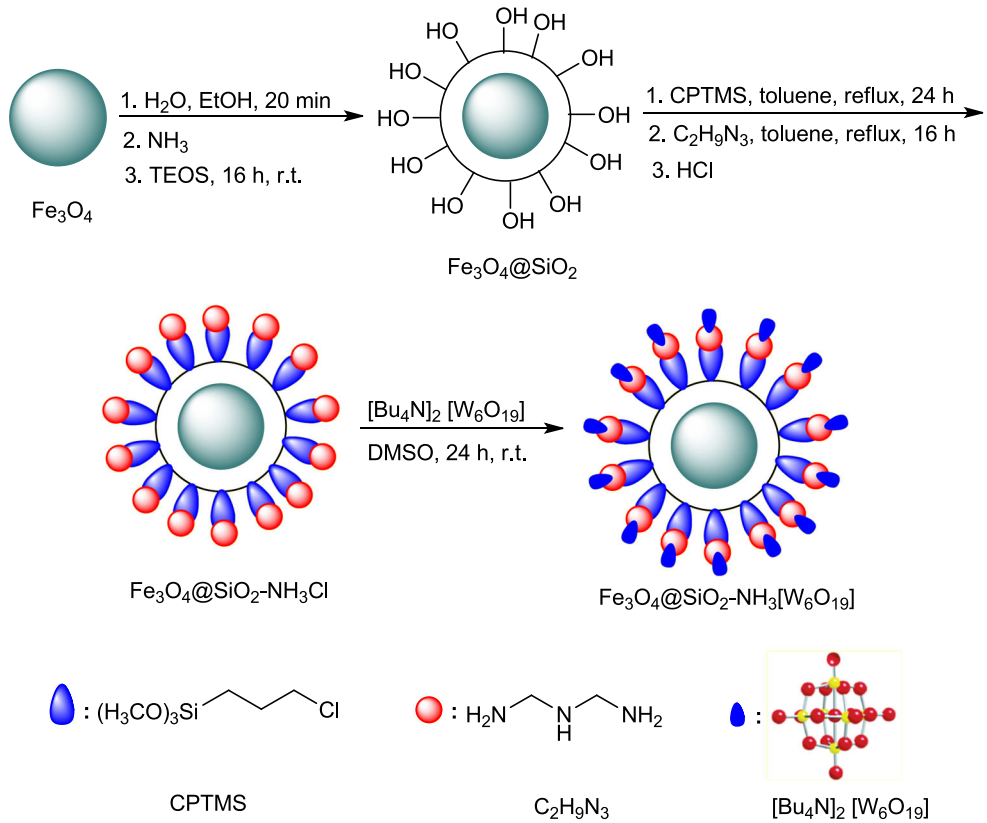

SCHEME 1 Preparation of the Fe_3O_4@SiO_2-NH_3[W_6O_{19}] nanocatalyst

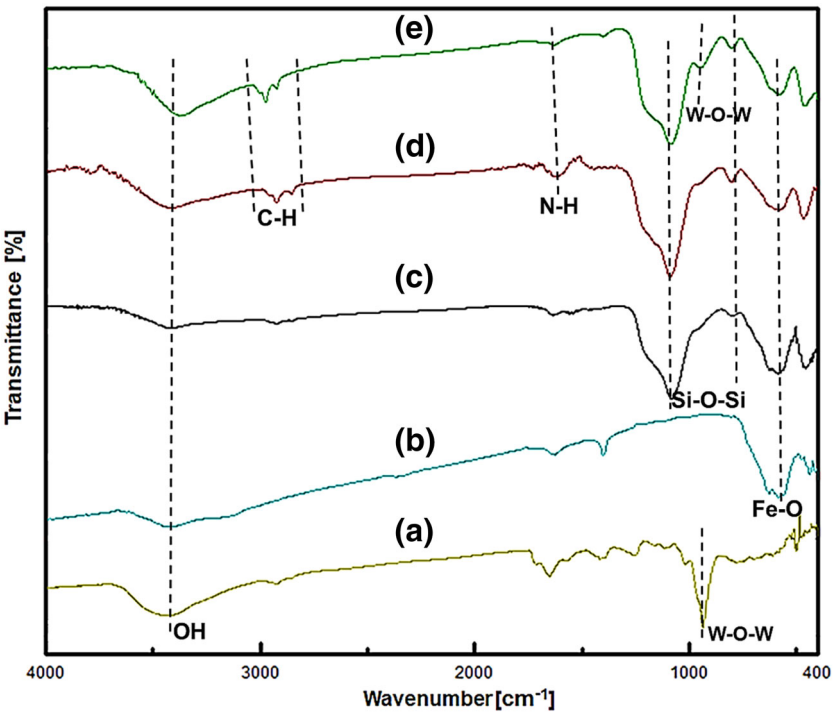

FIGURE 1 FT-IR spectra of (a) [Bu_4N]$_2$[W_6O_{19}], (b) Fe_3O_4, (c) Fe_3O_4@SiO_2, (d) Fe_3O_4@SiO_2-NH_3Cl, and (e) Fe_3O_4@SiO_2-NH_3[W_6O_{19}]

shell has attracted more attention.[38–40] It is also important to note that the Fe_3O_4 nanoparticles (NPs), prepared from easily available precursors and with tunable properties, have drawn much attention owing to their widespread applications in material and chemical processes.[41–43] Also, silica has received much attention due to its poor chemical permeability, non-toxicity, high chemical and thermal stability, and high availability of silanol groups on its surface for any modification.[26,44] Recently, different magnetic nanoparticles (MNPs) have been used as support for homogeneous catalysts. The most fascinating feature of MNP-supported catalysts is the easy recycling controlled by simple magnetically separation.[45–52] As example, a number of MNP-supported polyoxometalates have been prepared and applied as recoverable heterogeneous catalysts in organic reactions.[53,54] Some of the recent reports in this matter are γ-Fe_2O_3@SiO_2-PW,[55] magPOM-SILPs,[56] Fe_3O_4@SiO_2-HPW,[57] $BeW_{12}O_{40}$-ILSCCFNPs,[58] Fe@PILPW-AM,[19] and Fe_3O_4@SiO_2@HPW.[59]

In view of the above and in continuation of our recent studies in the fields of MNP-supported catalysts,[60–62] a Lindqvist-type polyoxometalate ($[Bu_4N]_2[W_6O_{19}]$) is immobilized on amine-modified Fe_3O_4@SiO_2 MNPs to deliver a powerful and highly recoverable catalyst for the synthesis of pyrazole derivatives.

2 | EXPERIMENTAL

2.1 | Synthesis of tetrabutylammonium hexatungstate salt ($[Bu_4N]_2[W_6O_{19}]$)

Lindqvist-type polyoxometalate ($[Bu_4N]_2[W_6O_{19}]$) was prepared according to a previous method.[63] For this, sodium tungstate dihydrate ($Na_2WO_4.2H_2O$, 1 g) was mixed with dimethylformamide (DMF, 0.9 ml) and acetic anhydride (1.2 ml) while incubating at 100°C for 4 h to give a white cream-like product. Then, HCl (0.6 ml, 12 N) and acetic anhydride (0.6 ml) and DMF (1.5 ml) were added to the reaction vessel. After 10 min, the mixture was filtered, washed with methanol, and allowed to cool to room temperature. Then, methanol (1.5 ml) and tetrabutylammonium bromide ($C_{16}H_{36}BrN$, 0.5 g) were added to the resulted mixture, and it was stirred for 10 min. The resulting precipitate was separated and washed with diethyl ether and methanol. Next, this material was added to dimethylsulfoxide (DMSO, 5 ml) and kept at 25°C for 1 day. Finally, the resulted mixture was filtered and dried under the vacuum condition. The resulted product was called $[Bu_4N]_2[W_6O_{19}]$.

2.2 | Synthesis of Fe_3O_4 NPs

The Fe_3O_4 NPs were prepared according to our previous procedure.[64] For this, firstly, $FeCl_3$·6H2O (3 g) and $FeCl_2$·4H2O (2 g) were dissolved in deionized water (25 ml). Then, NH_3 (20 ml, 25% wt) was added dropwise in the reaction mixture while stirring. The resulted combination was stirred at room temperature for 30 min.

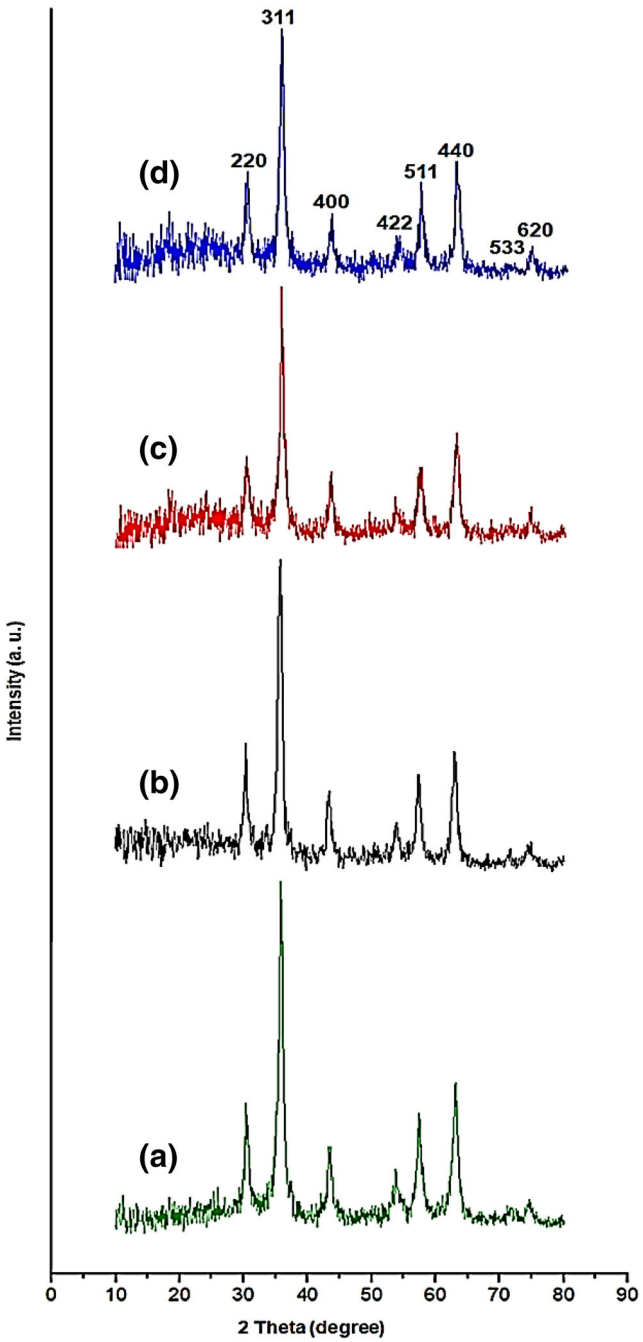

FIGURE 2 The wide-angle PXRD pattern of (a) Fe_3O_4, (b) Fe_3O_4@SiO_2, (c) Fe_3O_4@SiO_2-NH_3Cl, and (d) Fe_3O_4@SiO_2-$NH_3[W_6O_{19}]$

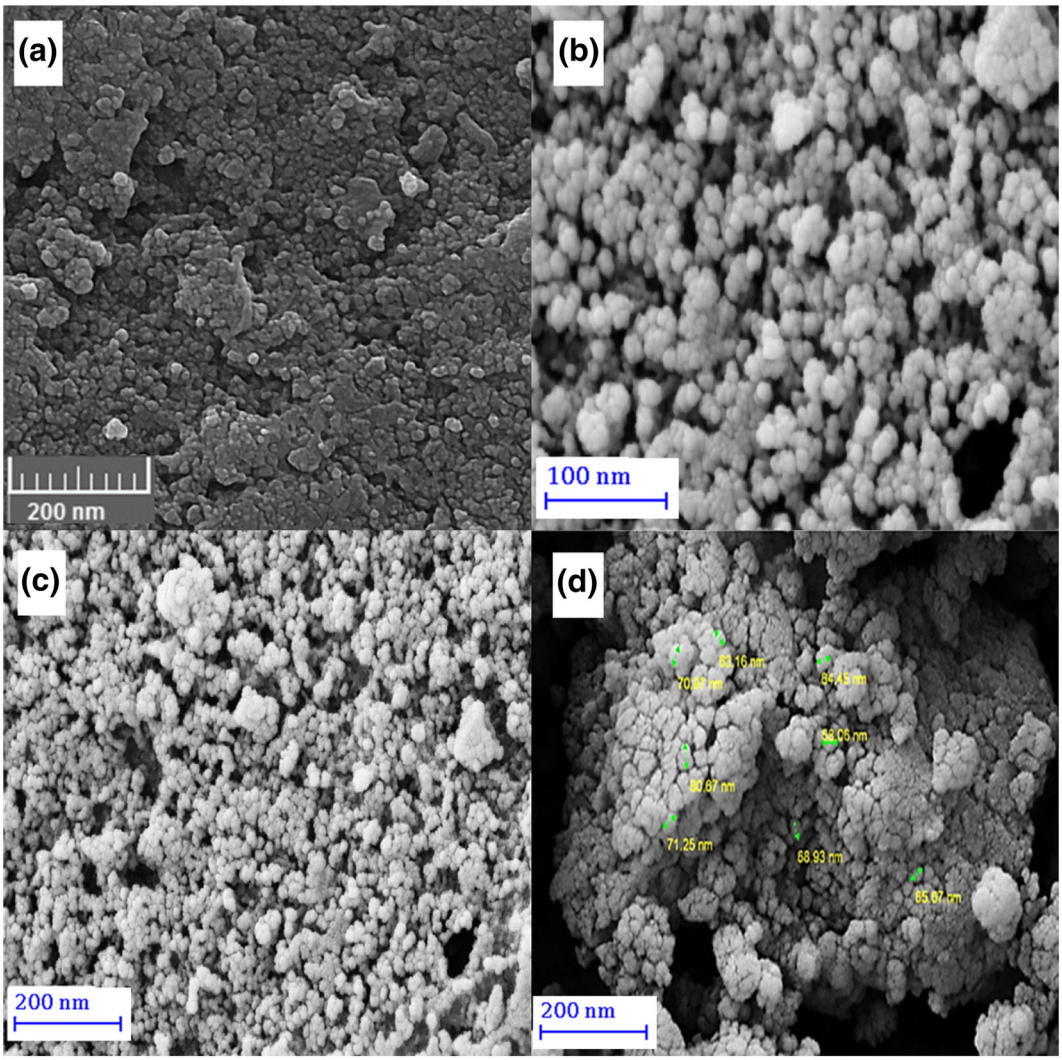

FIGURE 3 SEM image of (a) Fe_3O_4, (b) Fe_3O_4@SiO_2, (c) Fe_3O_4@SiO_2-NH_3Cl, and (d) Fe_3O_4@SiO_2-$NH_3[W_6O_{19}]$

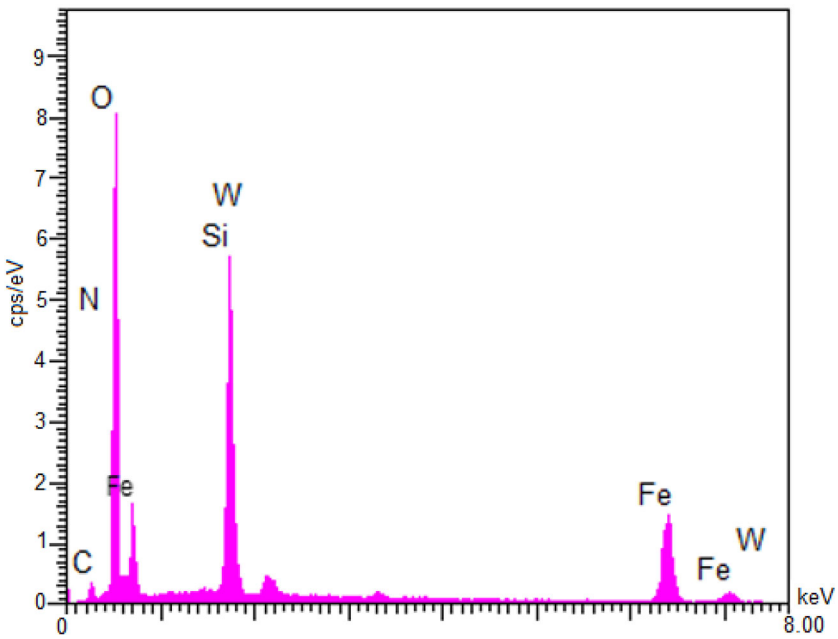

FIGURE 4 The EDX analysis of Fe_3O_4@SiO_2-$NH_3[W_6O_{19}]$

After that, the product was separated using an external magnet and washed with deionized water. The final material was dried at 70°C for 12 h and called Fe_3O_4 NPs.

2.3 | Synthesis of Fe_3O_4@SiO_2

For this purpose, the Fe_3O_4 NPs (0.5 g) were completely dispersed in a solution containing water (10 ml) and ethanol (40 ml) at room temperature for 20 min. After that, ammonia (4 ml, 25% wt) was added to the reaction vessel. Then, TEOS (0.5 ml) was added dropwise, and the resulted mixture was stirred at room temperature for 16 h. Next, the product was collected using a magnetic field and washed several times with ethanol and deionized water. The final material was dried at 70°C for 6 h and denoted as Fe_3O_4@SiO_2.

2.4 | Synthesis of Fe_3O_4@SiO_2-NH_3Cl

For this, 1 g of Fe_3O_4@SiO_2 was completely dispersed in toluene (30 ml) under ultrasonication. After 15 min, 3-chloropropyltrimethoxysilane (CPTMS, 1 mmol) was added in the vessel reaction, and this combination was refluxed for 24 h. Then, the product was collected using an external magnet, washed with ethanol and deionized water, dried at 70°C, and denoted as Fe_3O_4@SiO_2-PrCl. Subsequently, the Fe_3O_4@SiO_2-PrCl (1 g) was dispersed in toluene (40 ml). After adding of *N*-(aminomethyl)methanediamine (1.5 mmol), the mixture was refluxed for 16 h. Next, the resulted material was collected using a magnetic field and washed with ethanol and deionized water. Finally, the product was acidified with dilute HCl solution (40 ml, 0.5 M) to give Fe_3O_4@SiO_2-NH_3Cl.

2.5 | Immobilization of $[Bu_4N]_2[W_6O_{19}]$ on Fe_3O_4@SiO_2-NH_3Cl

For this, Fe_3O_4@SiO_2-NH_3Cl (1 g) was dispersed in DMSO (15 ml) under ultrasonication. Then, $[Bu_4N]_2[W_6O_{19}]$ (0.4 g) was added, and the resulted mixture was stirred at room temperature for 24 h. Next, the mixture was heated to 100°C and stirred at for 4 h. The final material was collected using a magnetic field and washed with ethanol and deionized water and dried in at 70°C for 7 h. The product was denoted as Fe_3O_4@SiO_2-$NH_3[W_6O_{19}]$.

2.6 | Procedure for the synthesis of pyrazole derivatives using Fe_3O_4@SiO_2-$NH_3[W_6O_{19}]$

For this purpose, Fe_3O_4@SiO_2-$NH_3[W_6O_{19}]$ (5 mg) was added to a flask containing malononitrile (1 mmol), aldehyde (1 mmol), phenylhydrazine (1 mmol), and ethanol (10 ml), and the resulted mixture was magnetically stirred at room temperature. The reaction progress was monitored by thin-layer chromatography (TLC). After completion of the process and removal of the catalyst, hot ethanol (8 ml) was added. Some ice species were finally added to the reaction vessel to precipitate the desired pyrazole products.

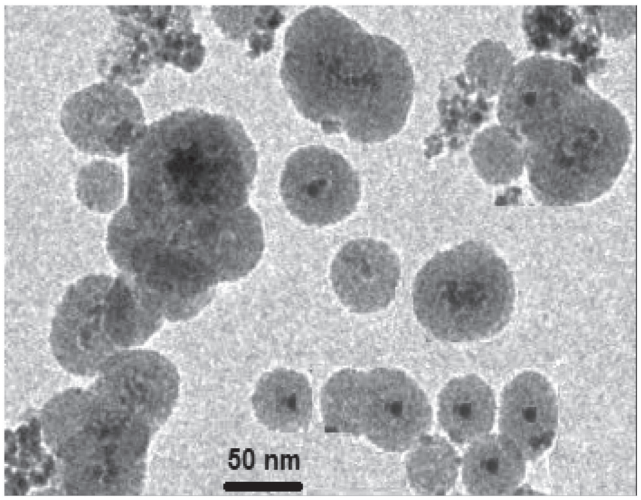

FIGURE 5 The TEM image of Fe_3O_4@SiO_2-$NH_3[W_6O_{19}]$

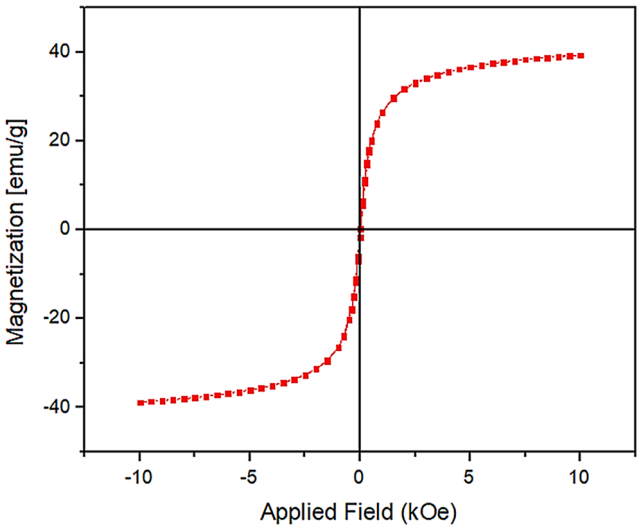

FIGURE 6 The VSM analysis of the Fe_3O_4@SiO_2-$NH_3[W_6O_{19}]$

3 | RESULTS AND DISCUSSION

The preparation of $Fe_3O_4@SiO_2$-$NH_3[W_6O_{19}]$ is illustrated in Scheme 1. As shown, a silica shell was first coated on the magnetite NPs through a sol–gel process to give $Fe_3O_4@SiO_2$. The $Fe_3O_4@SiO_2$ NPs were then modified with CPTMS and *N*-(aminomethyl)methanediamine ($C_2H_9N_3$) to deliver $Fe_3O_4@SiO_2$-NH_2. The $Fe_3O_4@SiO_2$-NH_2 material was acidified using a dilute HCl solution (2 M) to give $Fe_3O_4@SiO_2$-NH_3Cl. Finally, the $Fe_3O_4@SiO_2$-$NH_3[W_6O_{19}]$ was obtained via treatment of $Fe_3O_4@SiO_2$-NH_3Cl with $[Bu_4N]_2[W_6O_{19}]$ polyoxometalate.

The functional groups of the synthesized magnetic materials were determined using Fourier transform infrared (FT-IR) spectroscopy (Figure 1). The peak appeared at 530 cm^{-1} is related to Fe–O bond (Figure 1b–e).[44] The peak at 1655 cm^{-1} is assigned to bending and stretching vibrations of the N–H groups (Figure 1d,e). The peak observed at 3422 cm^{-1} is due to O–H bond (Figure 1a–e). The signals at 2825 and 2924 cm^{-1} are related to the vibrations of the C–H bonds of the propyl group (Figure 1d,e). The sharp peaks at 1070 and 823 cm^{-1} corresponded to the symmetric and asymmetric vibrations of Si–O–Si bonds of SiO_2 moieties (Figure 1c–e).[65] Also, the sharp peak at 800 cm^{-1} is related to the W-O-W vibrations (Figure 1a,e).[66] These results confirm successful incorporation/immobilization of magnetite core, silica moieties, and polyoxometalate complex into/onto material framework.

The wide-angle PXRD (WAPXRD) analysis of Fe_3O_4, $Fe_3O_4@SiO_2$, $Fe_3O_4@SiO_2$-NH_3Cl, and $Fe_3O_4@SiO_2$-$NH_3[W_6O_{19}]$ nanomaterials showed eight signals at 2θ of 30.49°, 35.78°, 43.39°, 53.87°, 57.38°, 62.91°, 74.63°, and 75.20°, respectively, corresponding to the Miller index values (*hkl*) of (220), (311), (400), (422), (511), (440), (533), and (620) (Figure 2).[60,67] These peaks are related to the crystalline structure of magnetic iron oxides, proving high stability and durability of these magnetite NPs during catalyst preparation steps.

Scanning electron microscopy (SEM) was performed to investigate the particle morphology at different steps of catalyst preparation. This clearly showed the presence of particles with spherical morphology and uniform size for the materials at all steps (Figure 3). In particular, the SEM of the $Fe_3O_4@SiO_2$-$NH_3[W_6O_{19}]$ clearly showed the presence of spherical particles with an average size of 68 nm (Figure 3d). These types of core-shell structured spherical particles are very good candidates for the adsorption and catalysis applications.

The chemical composition of $Fe_3O_4@SiO_2$-$NH_3[W_6O_{19}]$ was studied by energy-dispersive X-ray (EDX) spectroscopy (Figure 4). This analysis showed the presence of Fe (13.5%), W (1.9%), N (2.8%), Si (10.8%), C (9.1%), and O (61.6%) wt% elements in the sample, confirming the well incorporation/immobilization of expected species into/onto the material framework.

Figure 5 provides the transmission electron microscopy (TEM) image of the $Fe_3O_4@SiO_2$-NH_3 $[W_6O_{19}]$ catalyst. According to this analysis, a core-shell structure

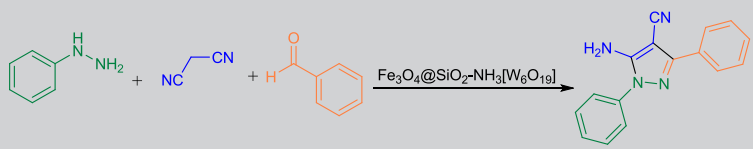

Entry	Solvent	Catalyst (mg)	Yield (%)[a]
1	-	5	42
2	Acetonitrile	5	79
3	Toluene	5	68
4	H_2O	5	85
5	EtOH	5	94
6	EtOH	3	80
7	EtOH	4	88
8	EtOH	6	91
9	EtOH	7	92

[a]All reactions were performed at room temperature for 25 min.

TABLE 1 Screening various parameters in the synthesis of pyrazoles catalyzed by $Fe_3O_4@SiO_2$-$NH_3[W_6O_{19}]$[a]

TABLE 2 Preparation of pyrazole derivatives in the presence of $Fe_3O_4@SiO_2$-$NH_3[W_6O_{19}]$ nanocatalyst[a]

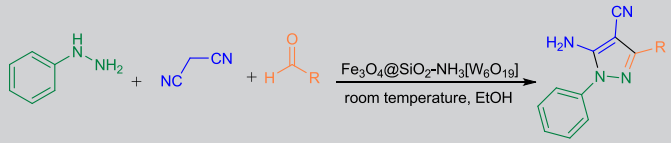

Entry	R	Time (min)	Yield (%)	M. P. (°C)	M. P. reported	Product
1		25	94	157–160	158–159[70]	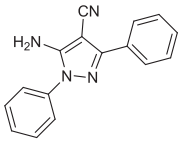
2		25	95	128–129	127–129[70]	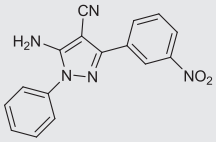
3	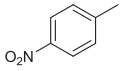	15	95	165–168	161–162[70]	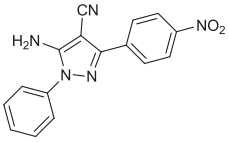
4	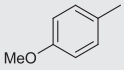	25	88	106–109	107–108[70]	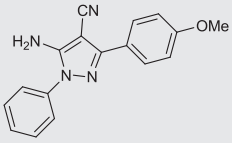
5	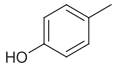	30	85	207–209	208–210[71]	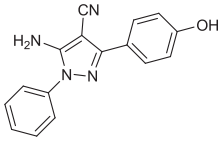
6	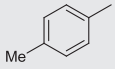	27	86	119–121	117–118[70]	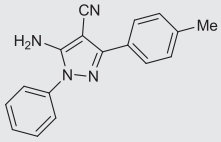

(Continues)

TABLE 2 (Continued)

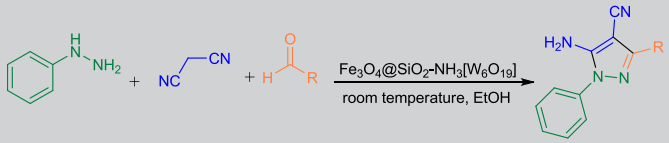

Entry	R	Time (min)	Yield (%)	M. P. (°C)	M. P. reported	Product
7		35	82	140–142	141–144[72]	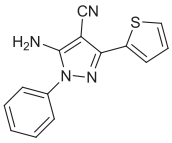
8[b]		40	74	128–130	128–129[73]	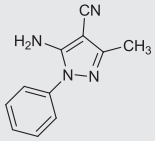

[a]Reaction conditions: aldehyde (1 mmol), malononitrile (1 mmol), phenylhydrazine (1 mmol), EtOH (5 ml), $Fe_3O_4@SiO_2$-$NH_3[W_6O_{19}]$ (5 mg), room temperature.
[b]2 mmol of aldehyde was used.

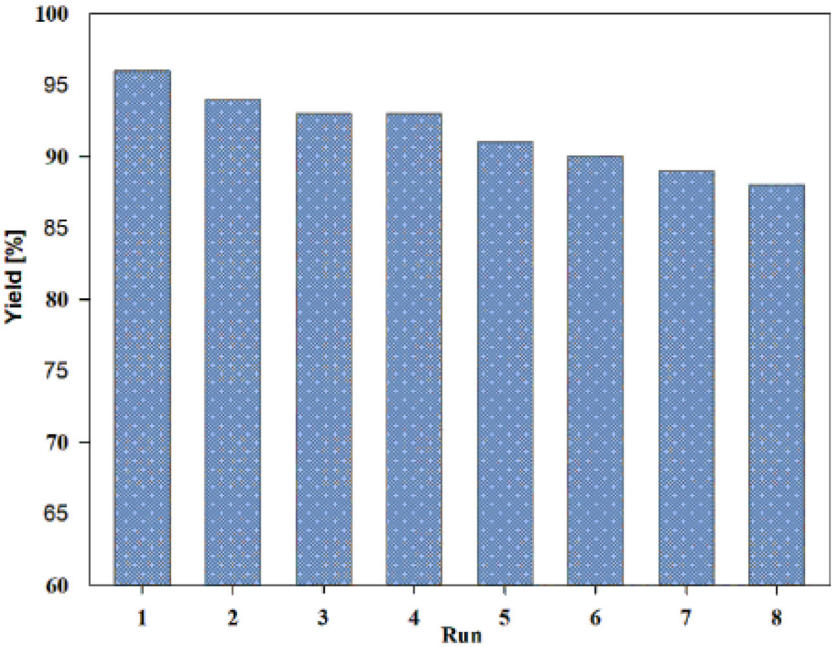

FIGURE 7 Reusability of $Fe_3O_4@SiO_2$-$NH_3[W_6O_{19}]$

with black core (magnetite NPs) and gray shell (modified silica layer) was confirmed for the designed catalyst.

The magnetic properties of $Fe_3O_4@SiO_2$-$NH_3[W_6O_{19}]$ were also studied using vibrating sample magnetometer (VSM) (Figure 6). As shown, a magnetization of about 38 emu/g is observed for the designed catalyst, confirming very good superparamagnetic behavior of the material that is a very important characteristic, especially in the field of catalytic application.[68,69]

After characterization of $Fe_3O_4@SiO_2NH_3[W_6O_{19}]$, its catalytic activity was studied in a multicomponent reaction to prepare pyrazole derivatives. The optimized condition was obtained in the reaction of benzaldehyde, phenylhydrazine, and malononitrile as a test model. For this, the effect of solvent and amount of catalyst were examined. Under solvent-free condition, only a low yield of the desired product was obtained (Table 1, Entry 1). In acetonitrile, toluene, and H_2O, respectively, 79%, 68%, and 85% yields were resulted (Table 1, Entries 2–4). The highest yield and conversion were obtained in ethanol (Table 1, Entry 5). It was also found that by increasing the catalyst amount from 3 to 5 mg, the yield is increased, and the further amount of catalyst has no notable effect on the reaction progress (Table 1, Entries 5–9). According to these results, the use of 5 mg of catalyst and ethanol as an environmentally friendly solvent at room temperature were selected as optimum conditions.

Under optimal conditions in hand, the efficiency of the designed catalyst in the synthesis of different derivatives of pyrazole was investigated (Table 2). As shown, all aromatic aldehydes bearing both electron-donating and electron-withdrawing substituents gave the corresponding pyrazole products in high yields (Table 2, Entries 1–6). The heteroaromatic substrates such as thiophene-2-carbaldehyde also delivered the pyrazole adduct in high yield (Table 2, Entry 7). The aliphatic aldehydes such as ethanal also gave corresponding pyrazole in good yield (Table 2, Entry 8). These results confirm high performance of the designed catalyst to

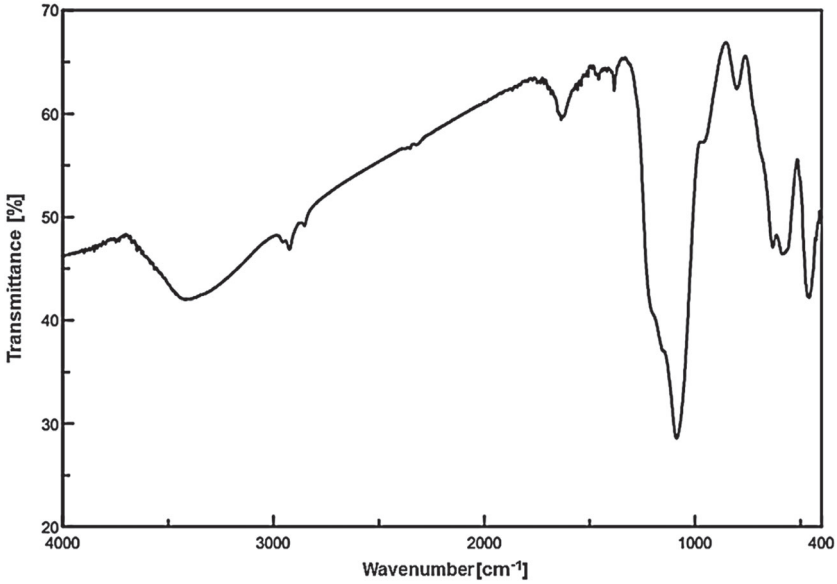

FIGURE 8 FT-IR spectrum of the recovered $Fe_3O_4@SiO_2$-$NH_3[W_6O_{19}]$ catalyst

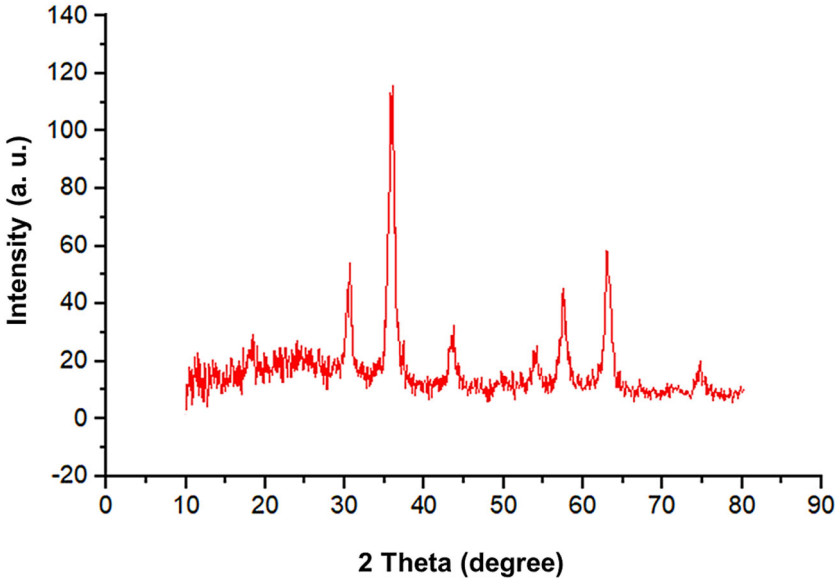

FIGURE 9 PXRD pattern of the recovered $Fe_3O_4@SiO_2$-$NH_3[W_6O_{19}]$ catalyst

prepare a wide range of biologically active pyrazole derivatives.

After that, the reusability and recoverability of the catalytic system were investigated. To do this, the condensation between malononitrile, benzaldehyde, and phenylhydrazine in the presence of the Fe_3O_4@SiO_2-$NH_3[W_6O_{19}]$ nanocatalyst was selected as a test model. For this, after the end of each run, the catalyst was separated using a magnetic field and reused in another cycle under conditions the same as the first run. The results showed that the Fe_3O_4@SiO_2-$NH_3[W_6O_{19}]$ catalyst can be reused and recovered at least seven times without a significant loss in its performance (Figure 7). This confirms high durability and high stability of the designed catalyst under applied conditions.

To confirm the chemical and structural stability of the nanocatalyst during eight runs of use, the recovered catalyst was characterized by the FT-IR, powder X-ray diffraction (PXRD), VSM, SEM, and TEM analyses. The FT-IR pattern of the recovered catalyst was the same as the FT-IR spectrum of the fresh catalyst, proving the high chemical stability of the Fe_3O_4@SiO_2-$NH_3[W_6O_{19}]$ catalyst under applied conditions (Figure 8).

As shown in Figure 9, the pattern of PXRD analysis of the recovered catalyst is also the same as the PXRD pattern of the fresh catalyst, confirming high stability of the crystalline structure of the Fe_3O_4 NPs during the recovery times.

The magnetic properties of the recovered catalyst were investigated by VSM analysis (Figure 10). The result showed that the recovered catalyst has the same superparamagnetic behavior as the fresh catalyst and its magnetic saturation did not change significantly during the reaction conditions.

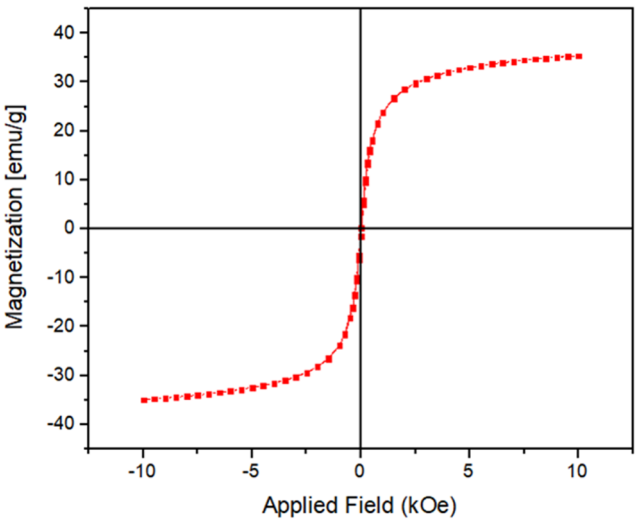

FIGURE 10 VSM analysis of the recovered Fe_3O_4@SiO_2-$NH_3[W_6O_{19}]$ catalyst

The SEM image of the recovered catalyst also showed a uniform spherical structure the same as its fresh parent, confirming high stability of the material structure during applied conditions (Figure 11).

The TEM image of the recovered catalyst was also performed and compared with that of fresh catalyst (Figure 12). As shown, the same as fresh catalyst, the TEM image of the recovered catalyst also shows a core-shell structure, proving the high stability of the material structure during applied conditions.

In the next step, a leaching test was carried out to study the heterogeneous behavior of the designed

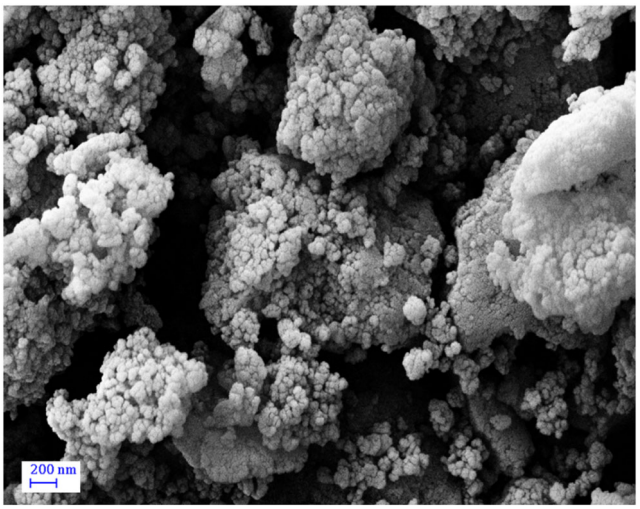

FIGURE 11 The SEM image of the recovered Fe_3O_4@SiO_2-$NH_3[W_6O_{19}]$ catalyst

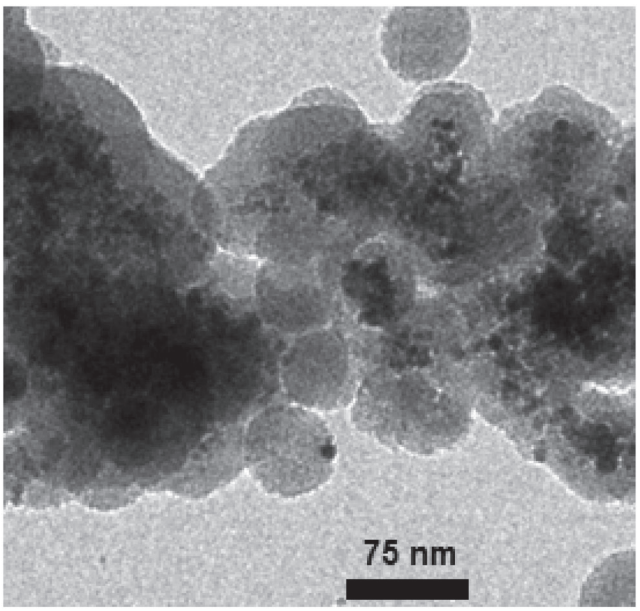

FIGURE 12 The TEM image of the recovered Fe_3O_4@SiO_2-$NH_3[W_6O_{19}]$ catalyst

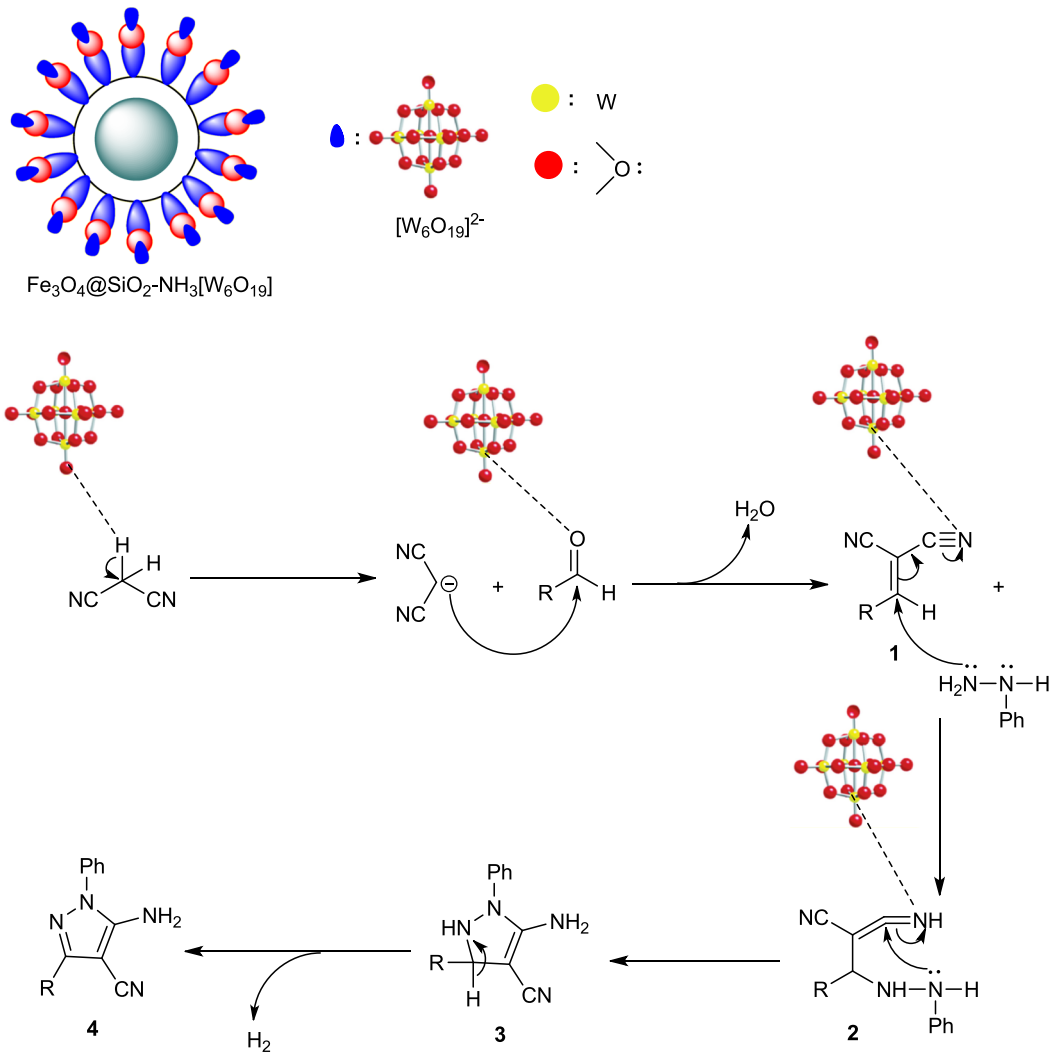

SCHEME 2 Proposed mechanism for the synthesis of 5-amino-1,3-diphenyl-1*H*-pyrazole-4-carbonitrile derivatives using Fe_3O_4@SiO_2-$NH_3[W_6O_{19}]$ catalyst

TABLE 3 A comparison study between performance of Fe_3O_4@SiO_2-$NH_3[W_6O_{19}]$ and former catalysts in the synthesis of pyrazoles

Entry	Catalyst	Conditions	Time (min)	Recovery times	Ref.
1	Fe_3O_4	H_2O, r.t	60	6	[74]
2	Alumina-silica-MnO_2/SDBS	Distilled water, 35°C	3	5	[70]
3	Glu.@Fe_3O_4	H_2O, r.t.	8	4	[75]
4	Fe_3O_4@CQDs@Si $(CH_2)_3NH_2$@CC@EDA@Cu	Solvent-free, r.t.	5	4	[72]
5	Fe_3O_4@SiO_2-N$[W_6O_{19}]$	EtOH, r.t.	25	7	This work

catalyst. For this, after completion of about 40% of the condensation process, the catalyst was removed using a magnet, and the progress of the residue mixture was monitored. Interestingly, after 50 min, no significant progress was observed in the reaction, implying the effectiveness of the Fe_3O_4@SiO_2-NH_3Cl support in the well immobilization of active hexatungstate species.

A mechanism for the synthesis of 5-amino-1,-3-diphenyl-1*H*-pyrazole-4-carbonitrile derivatives using Fe_3O_4@SiO_2-$NH_3[W_6O_{19}]$ catalyst is proposed in Scheme 2. In the first step, the acidic proton of malononitrile is deprotonated by Lewis basic oxygen groups of the catalyst, and the corresponding anion is produced. Then, this anion is condensed with the W-

activated aldehyde through a Knoevenagel process to deliver intermediate **1**. In the next step, the intermediate **1**, as a Michael acceptor, reacts with the phenylhydrazine to give intermediate **2**. After that, intermediate **2** is converted to intermediate **3** through an intramolecular cyclocondensation. Finally, the desired product **4** is formed through oxidation and releasing a hydrogen molecule ($-H_2$).[70,71]

Finally, the catalytic performance of our designed catalyst was compared with some of the catalysts recently used in the preparation of pyrazoles. This study showed that present catalyst is better than of the previous catalysts in recycling times and reaction time. Also, this study confirmed the higher efficiency and stability of the present catalyst compared with previous catalytic systems (Table 3).

4 | CONCLUSION

A novel core-shell structured magnetite silica-supported hexatungstate (Fe_3O_4@SiO_2-$NH_3[W_6O_{19}]$) nanocatalyst was prepared, and its properties were investigated. The FT-IR and EDX analyses of the Fe_3O_4@SiO_2-$NH_3[W_6O_{19}]$ proved the well immobilization/incorporation of hexatungstate ions and silica shell on the surface of the Fe_3O_4 NPs. The SEM and TEM images showed spherical particles with core-shell structure for the catalyst. The PXRD and VSM analyses confirmed good magnetic properties of the Fe_3O_4@SiO_2-$NH_3[W_6O_{19}]$ nanocatalyst. This catalyst was heterogeneously and effectively employed in the synthesis of pyrazole derivatives under green conditions. Other advantages of this catalytic system were the use of low catalyst loading, short reaction times, the use of green solvent at RT, high stability, and easy recoverability of catalyst under applied conditions.

ACKNOWLEDGMENTS

The authors thank the Yasouj University and the Iran National Science Foundation (INSF) for supporting this work.

AUTHOR CONTRIBUTIONS

Ramin Nemati: Investigation; software. **Dawood Elhamifar:** Conceptualization; data curation; project administration. **Ali Zarnegaryan:** Formal analysis; software. **Masoumeh Shaker:** Formal analysis; software.

DATA AVAILABILITY STATEMENT

The data that support the findings of this study are available from the corresponding author upon reasonable request.

ORCID

Ramin Nemati https://orcid.org/0000-0002-0800-1433
Dawood Elhamifar https://orcid.org/0000-0003-4889-9505
Ali Zarnegaryan https://orcid.org/0000-0001-8630-0335
Masoumeh Shaker https://orcid.org/0000-0001-8216-2238

REFERENCES

[1] A. Ansari, A. Ali, M. Asif, *New J. Chem.* **2017**, *41*, 16.
[2] S. Fustero, M. Sanchez-Rosello, P. Barrio, A. Simon-Fuentes, *Chem. Rev.* **2011**, *111*, 6984.
[3] Y. Kaddouri, F. Abrigach, E. B. Yousfi, M. El Kodadi, R. Touzani, *Heliyon* **2020**, *6*, e03185.
[4] A. Tanitame, Y. Oyamada, K. Ofuji, M. Fujimoto, N. Iwai, Y. Hiyama, K. Suzuki, H. Ito, H. Terauchi, M. Kawasaki, *J. Med. Chem.* **2004**, *47*, 3693.
[5] M. Parshad, V. Verma, D. Kumar, *Monatash. Chem.* **2014**, *145*, 1857.
[6] A. Vijesh, A. M. Isloor, P. Shetty, S. Sundershan, H. K. Fun, *Eur. J. Med. Chem.* **2013**, *62*, 410.
[7] H. Dai, S. Ge, J. Guo, S. Chen, M. Huang, J. Yang, S. Sun, Y. Ling, Y. Shi, *Eur. J. Med. Chem.* **2018**, *143*, 1066.
[8] A. Titi, M. Messali, B. A. Alqurashy, R. Touzani, T. Shiga, H. Oshio, M. Fettouhi, M. Rajabi, F. A. Almalki, T. B. Hadda, *J. Mol. Struct.* **2020**, *1205*, 127625.
[9] D. Raffa, B. Maggio, M. V. Raimondi, S. Cascioferro, F. Plescia, G. Cancemi, G. Daidone, *Eur. J. Med. Chem.* **2015**, *97*, 732.
[10] D. Kaushik, S. A. Khan, G. Chawla, S. Kumar, *Eur. J. Med. Chem.* **2010**, *45*, 3943.
[11] K. Karrouchi, S. Radi, Y. Ramli, J. Taoufik, Y. N. Mabkhot, F. A. Al-Aizari, *Molecules* **2018**, *23*, 134.
[12] Y. Ding, T. Zhang, Q.-Y. Chen, C. Zhu, *Org. Lett.* **2016**, *18*, 4206.
[13] D. L. Long, R. Tsunashima, L. Cronin, *Angew. Chem., Int. Ed.* **2010**, *49*, 1736.
[14] A. Pearson, S. K. Bhargava, V. Bansal, *Langmuir* **2011**, *27*, 9245.
[15] A. Pearson, H. Zheng, K. Kalantar-Zadeh, S. K. Bhargava, V. Bansal, *Langmuir* **2012**, *28*, 14470.
[16] A. Pearson, S. Bhosale, S. K. Bhargava, V. Bansal, *ACS Appl. Mater. Interfaces* **2013**, *5*, 7007.
[17] X. López, J. J. Carbó, C. Bo, J. M. Poblet, *Chem. Soc. Rev.* **2012**, *41*, 7537.
[18] F. Bentaleb, O. Makrygenni, D. Brouri, C. Coelho Diogo, A. Mehdi, A. Proust, F. Launay, R. Villanneau, *Inorg. Chem.* **2015**, *54*, 7607.
[19] Y. Leng, J. Zhao, P. Jiang, J. Wang, *ACS Appl. Mater. Interfaces* **2014**, *6*, 5947.
[20] C. Yvon, A. J. Surman, M. Hutin, J. Alex, B. O. Smith, D. L. Long, L. Cronin, *Am. Ethnol.* **2014**, *126*, 3404.
[21] Y.-F. Song, R. Tsunashima, *Chem. Soc. Rev.* **2012**, *41*, 7384.
[22] A. Proust, B. Matt, R. Villanneau, G. Guillemot, P. Gouzerh, G. Izzet, *Chem. Soc. Rev.* **2012**, *41*, 7605.
[23] A. Proust, R. Thouvenot, P. Gouzerh, *Chem. Commun.* **2008**, 1837.
[24] Y.-C. Wang, X.-Y. Liu, X.-X. Wang, M.-S. Cao, *Chem. Eng. J.* **2021**, *419*, 129459.

[25] Y. Chen, L. Wang, W. Wang, M. Cao, *Appl. Catal. B* **2017**, *209*, 110.
[26] M. Shaker, D. Elhamifar, *Compos. Commun.* **2021**, *24*, 100608.
[27] Z. Hajizadeh, F. Radinekiyan, R. Eivazzadeh-Keihan, A. Maleki, *Sci. Rep.* **2020**, *10*, 1.
[28] A. Kozlovskiy, I. Kenzhina, M. Zdorovets, *Ceram. Int.* **2020**, *46*, 10262.
[29] S. Alla, A. Verma, V. Kumar, R. Mandal, I. Sinha, N. Prasad, *RSC Adv.* **2016**, *6*, 61927.
[30] M. Nasrollahzadeh, Z. Issaabadi, S. M. Sajadi, *Sep. Purif. Technol.* **2018**, *197*, 253.
[31] M. Baghayeri, E. N. Zare, R. Hasanzadeh, *Mater. Sci. Eng. C* **2014**, *39*, 213.
[32] Z. Ramazani, D. Elhamifar, M. Norouzi, R. Mirbagheri, *Compos. B. Eng.* **2019**, *164*, 10.
[33] M. Norouzi, D. Elhamifar, *Compos. B. Eng.* **2019**, *176*, 107308.
[34] F. Wu, J. T. Lee, E. Zhao, B. Zhang, G. Yushin, *ACS Nano* **2016**, *10*, 1333.
[35] M. Razavi, M. Fathi, M. Meratian, *Mater. Charact.* **2010**, *61*, 1363.
[36] Q. Cheng, D. Ye, W. Yang, S. Zhang, H. Chen, C. Chang, L. Zhang, *ACS Sustainable Chem. Eng.* **2018**, *6*, 8040.
[37] A. Trajcheva, N. Politakos, B. T. Pérez, Y. Joseph, J. B. Gilev, R. Tomovska, *Polymer* **2021**, *213*, 123335.
[38] Y. Chi, Q. Yuan, Y. Li, J. Tu, L. Zhao, N. Li, X. Li, *J. Colloid Interface Sci.* **2012**, *383*, 96.
[39] M. Stjerndahl, M. Andersson, H. E. Hall, D. M. Pajerowski, M. W. Meisel, R. S. Duran, *Langmuir* **2008**, *24*, 3532.
[40] X. Guo, F. Mao, W. Wang, Y. Yang, Z. Bai, *ACS Appl. Mater. Interfaces* **2015**, *7*, 14983.
[41] S. Si, C. Li, X. Wang, D. Yu, Q. Peng, Y. Li, *Cryst. Growth des.* **2005**, *5*, 391.
[42] Y. S. Kang, S. Risbud, J. F. Rabolt, P. Stroeve, *Chem. Mater.* **1996**, *8*, 2209.
[43] J. Sun, S. Zhou, P. Hou, Y. Yang, J. Weng, X. Li, M. Li, *J. Biomed. Mater. Res. A* **2007**, *80*, 333.
[44] M. Shaker, D. Elhamifar, *Front. Energy Res.* **2020**, *8*, 78.
[45] R. Sharma, Y. Monga, A. Puri, *J. Mol. Catal. A: Chem.* **2014**, *393*, 84.
[46] W. Xie, H. Wang, *Renewable Energy* **2020**, *145*, 1709.
[47] K. Bhaduri, B. D. Das, R. Kumar, S. Mondal, S. Chatterjee, S. Shah, J. J. Bravo-Suárez, B. Chowdhury, *ACS Omega* **2019**, *4*, 4071.
[48] P. Mofatehnia, G. M. Ziarani, D. Elhamifar, A. Badiei, *J. Phys. Chem. Solids* **2021**, *155*, 110097.
[49] A. R. Sardarian, I. D. Inaloo, M. Zangiabadi, *New J. Chem.* **2019**, *43*, 8557.
[50] I. D. Inaloo, S. Majnooni, H. Eslahi, M. Esmaeilpour, *Mol. Catal.* **2020**, *492*, 110915.
[51] I. Dindarloo Inaloo, S. Majnooni, H. Eslahi, M. Esmaeilpour, *Appl. Organomet. Chem.* **2020**, *34*, e5662.
[52] I. D. Inaloo, S. Majnooni, *Eur. J. Org. Chem.* **2019**, *2019*, 6359.
[53] H. Hamadi, M. Kooti, M. Afshari, Z. Ghiasifar, N. Adibpour, *J. Mol. Catal. A: Chem.* **2013**, *373*, 25.
[54] X. Zheng, L. Zhang, J. Li, S. Luo, J.-P. Cheng, *Chem. Commun.* **2011**, *47*, 12325.
[55] E. Rafiee, S. Eavani, *Green Chem.* **2011**, *13*, 2116.
[56] A. Misra, C. Zambrzycki, G. Kloker, A. Kotyrba, M. H. Anjass, I. Franco Castillo, S. G. Mitchell, R. Güttel, C. Streb, *Angew. Chem., Int. Ed.* **2020**, *59*, 1601.
[57] S. Wang, Z. Zhang, B. Liu, J. Li, *Catal. Sci. Technol.* **2013**, *3*, 2104.
[58] A. Amiri, H. R. Saadati-Moshtaghin, F. M. Zonoz, *Microchim. Acta* **2018**, *185*, 1.
[59] Y. Hou, J. Ma, T. Wang, Q. Fu, *Mater. Sci. Semicond. Process.* **2015**, *39*, 229.
[60] S. Kargar, D. Elhamifar, A. Zarnegaryan, *J. Phys. Chem. Solids* **2020**, *146*, 109601.
[61] M. Neysi, A. Zarnegaryan, D. Elhamifar, *New J. Chem.* **2019**, *43*, 12283.
[62] A. Zarnegaryan, M. Moghadam, S. Tangestaninejad, V. Mirkhani, I. Mohammadpoor-Baltork, *Polyhedron* **2016**, *115*, 61.
[63] M. Fournier, W. Klemperer, *Inorg. Synth.* **1990**, *27*, 81.
[64] R. Mirbagheri, D. Elhamifar, *J. Alloys Compd.* **2019**, *790*, 783.
[65] R. K. Sodhi, S. Paul, J. Clark, *Green Chem.* **2012**, *14*, 1649.
[66] M. Sarma, T. Chatterjee, S. K. Das, *Dalton Trans.* **2011**, *40*, 2954.
[67] S. Xuan, Y.-X. J. Wang, J. C. Yu, K. Cham-Fai Leung, *Chem. Mater.* **2009**, *21*, 5079.
[68] X. Li, H. Zhu, J. Feng, J. Zhang, X. Deng, B. Zhou, H. Zhang, D. Xue, F. Li, N. J. Mellors, *Carbon* **2013**, *60*, 488.
[69] H. Wang, X. Yuan, Y. Wu, X. Chen, L. Leng, H. Wang, H. Li, G. Zeng, *Chem. Eng. J.* **2015**, *262*, 597.
[70] R. Singh, *Res. Chem. Intermed.* **2019**, *45*, 4531.
[71] H. Kiyani, M. Bamdad, *Res. Chem. Intermed.* **2018**, *44*, 2761.
[72] N. Sarmasti, J. Y. Seyf, A. Khazaei, *Arab. J. Chem.* **2021**, *14*, 103026.
[73] H. Beyzaei, M. Moghaddam-Manesh, R. Aryan, B. Ghasemi, A. Samzadeh-Kermani, *Chem. Pap.* **2017**, *71*, 1685.
[74] M. A. E. A. A. Ali, *Tetrahedron* **2014**, *70*, 2971.
[75] N. Esfandiary, A. Nakisa, K. Azizi, J. Azarnia, I. Radfar, A. Heydari, *Appl. Organomet. Chem.* **2017**, *31*, e3641.

How to cite this article: R. Nemati, D. Elhamifar, A. Zarnegaryan, M. Shaker, *Appl Organomet Chem* **2021**, e6409. https://doi.org/10.1002/aoc.6409